STUDY OF SURFACE FIELD ENHANCEMENTS DUE TO FINE STRUCTURES

Tetsuo ABE[*]

High Energy Accelerator Research Organization (KEK)
1-1 Oho, Tsukuba, Ibaraki 305-0801, Japan

Abstract

High-gradient accelerating structures are linchpins of high-energy accelerators to search for new physics in particle physics. In this paper, local surface-field enhancements at fine concave structures, which could deteriorate performance of such accelerators, are numerically calculated with three different methods, including floating random walk.

INTRODUCTION

High-gradient radio-frequency (RF) accelerating structures are linchpins of high-energy accelerators to search for new physics in particle physics. However, fine surface defects in the structures, such as burrs from machining and undulations due to crystal structures, could increase surface fields and/or surface heating, and trigger breakdown of the accelerating structures, leading to deterioration of accelerator performance.

As is well known, projection tips, or similar fine structures, can dramatically increase local surface fields. On the other hand, how much is field enhancement at fine concave structures? Such structures could be made at bonding planes, e.g. of quadrant-type X-band accelerating structures for CLIC [1]. This is a problem presented in this paper, and surface-field enhancement factors are numerically calculated with three different methods: RF- and electrostatic-field simulations based on the Finite Integration Technique (FIT; e.g. see [2]), and floating random walk.

GEOMETRY OF CONCAVE STRUCTURE

Surface-field enhancements are calculated for a concave structure, parametrizing it by three parameters: R, G, and Δ, as shown in Fig. 1. The value of R is fixed to be $50\mu m$, simulating the $R = 50\,\mu m$ round chamfer on the edges of the bonding planes of the quadrant-type X-band accelerating structures for CLIC [1]. The values of G and Δ are floated in the following simulations.

The X-axis is always defined, as shown in Fig. 1, with its origin located at the center of the gap.

In this study, there is only one material of a conductor, which is treated as perfect electric conductor (PEC).

_____
[*] tetsuo.abe@kek.jp

METHOD1: FIT-BASED RF-FIELD SIMULATION

Assuming X-band accelerating structures, a port mode of TE_{10} with a cutoff frequency of $10\,GHz$ is computed for a rectangular waveguide with a size of $a = 15\,mm$ and $b = 1.0\,mm$, as shown in Fig.2, where there is a small groove of the concave structure at the center of the E-plane. Field enhancement factors are calculated as a ratio of the maximum field strength around the round chamfer (E_{max}) and the reference field strength at $X = 0$ on the E-plane in the opposite side (E_{ref}), i.e. E_{max}/E_{ref}.

For port mode computations, `CST MICROWAVE STUDIO` (`MWS`) [3, 4] is used, which is based on the FIT, a generalized finite-difference scheme for the solution of Maxwell's equations. We adopt hexahedral meshing with an advanced curved-boundary approximation [5], where a parameter on the number of mesh lines per wavelength is increased to 300 from its default value of 10, leading to a mesh size of about $100\,\mu m$ at the points far from the groove. Furthermore, another meshing parameter on the automatic mesh refinement at curved surfaces (RAPL) is increased to 5 from its default value of 2. Figure 3 shows how the meshing changes as the parameter RAPL is increased. Figure 4-(a) shows an example of the electric-field strength around the round chamfer. As shown in Fig. 4-(b), the surface electric-field strength (E_{surf}) as a function of X is more continuous with RAPL=5 than RAPL=2, and the maximum field strengths are almost the same, so that we adopt this meshing with RAPL=5 in this study.

Figure 5-(a) shows computation results as functions of G and Δ. There is at least 20% enhancement even though there is no gap and $\Delta = 0$ for the $R = 50\mu m$ round cham-
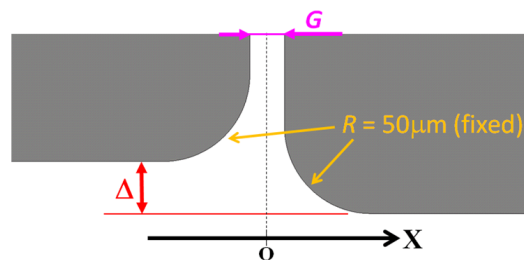

Figure 1: Parametrization of a concave structure. The gray and white areas indicate PEC and vacuum regions, respectively.
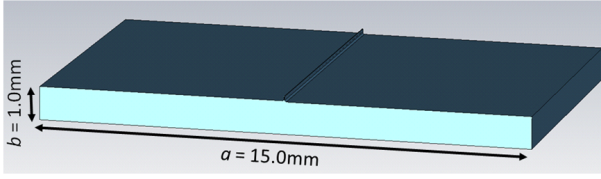
Figure 2: Vacuum region of the rectangular waveguide with a small groove at the center of the E-plane. The background material is PEC.
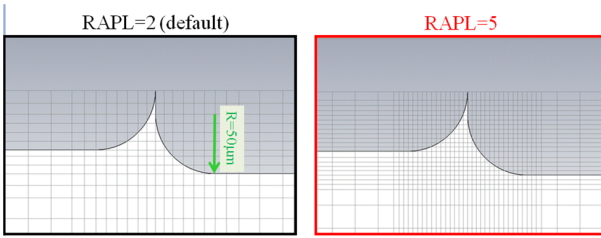

Figure 3: Hexahedral meshing around the round chamfer in the case of $G = 0$ and $\Delta = 20\mu$m by MWS.

fer. The electric field could be enhanced by 40% if the Δ becomes around 25μm.

METHOD2: FIT-BASED STATIC-FIELD SIMULATION

If the size of the fine structure is much smaller than the wavelength of the RF field, local fields near the fine structure can be calculated as static fields. In this section, electrostatic fields are calculated by using CST EM STUDIO (EMS) [3, 4], which is also based on the FIT, for the geometry shown in Fig. 6, where the meshing conditions are the same as in the previous section. The distance and potential difference between the two plates are set to be $b = 1.0$ mm and 1.0 V, respectively. Field enhancement factors are calculated as a ratio of the maximum field strength around the round chamfer ($E_{\max}$) and 1000 V/m, i.e. $E_{\max}/(1000\,\text{V/m})$.

Figure 5-(b) shows computation results as functions of G and Δ. There are very good agreements between the RF (Figure 5-(a)) and electrostatic (Figure 5-(b)) computations as expected.

METHOD3: FLOATING RANDOM WALK (FRW)

While the above-mentioned two methods are based on deterministic algorithms with space discretization, the FRW method (e.g. see [6]) is a stochastic approach without space discretization. It is based on the following formula to calculate an electrostatic potential ϕ in the case of no true
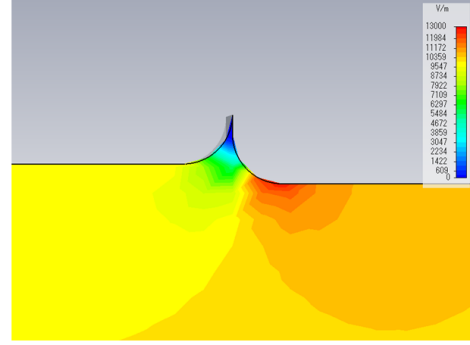
(a) Distribution of the electric-field strength computed with $RAPL = 5$.
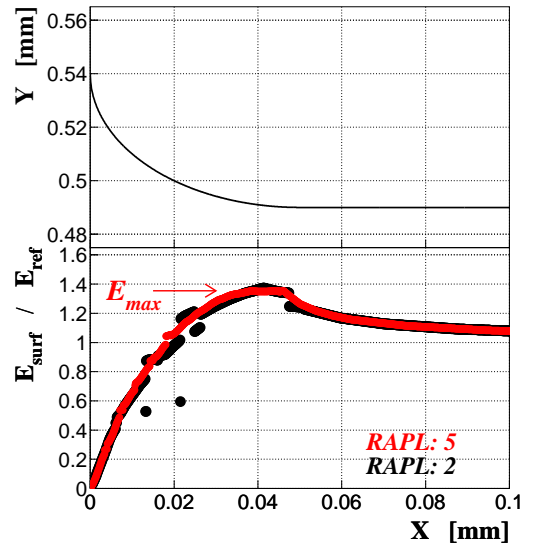
(b) Conductor surface (top) and the surface electric-field strength as a function of X computed with a RAPL value of 2 (black) or 5 (red) (bottom).

Figure 4: Example of the results of the port-mode computations using MWS in the case of $G = 0$ and $\Delta = 20\,\mu$m.

charge [7]:

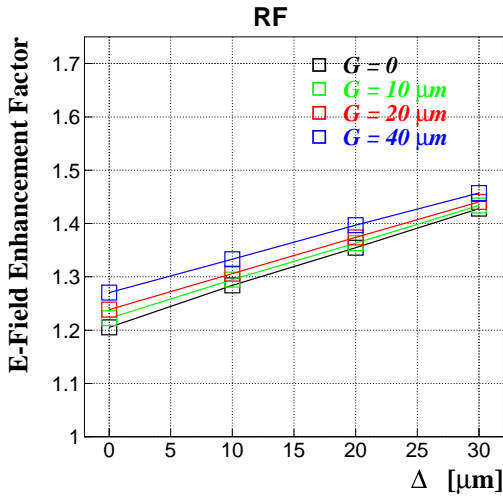$$\phi(X,Y) = \frac{1}{2\pi r_1}\oint_{C_1} ds_1\, \phi(X_1,Y_1) \quad (1)$$

$$= \frac{1}{2\pi r_1}\oint_{C_1} ds_1 \frac{1}{2\pi r_2}\oint_{C_2} ds_2\, \phi(X_2,Y_2) \quad (2)$$

$$= \frac{1}{2\pi r_1}\oint_{C_1} ds_1 \frac{1}{2\pi r_2}\oint_{C_2} ds_2 \cdots$$
$$\cdots \frac{1}{2\pi r_N}\oint_{C_N} ds_N\, \phi(X_N,Y_N)\,, \quad (3)$$
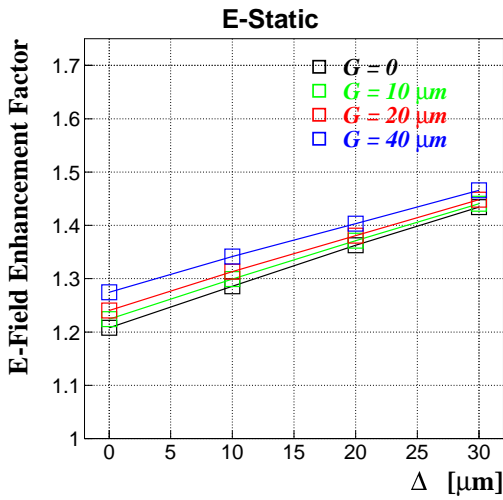
where C_l indicates a circle with a fixed radius of r_l:

$$r_l = \sqrt{X_l^2 + Y_l^2}\,, \quad (4)$$

and the value of r_l ($l = 1, 2, \cdots, N$) is always set to be the minimum distance to the boundary with a known potential. In the FRW method, a probabilistic interpretation is given

(a) For RF fields computed by using `MWS`.

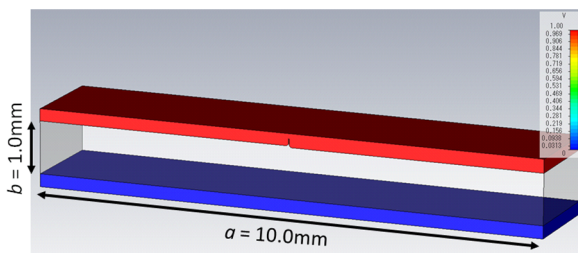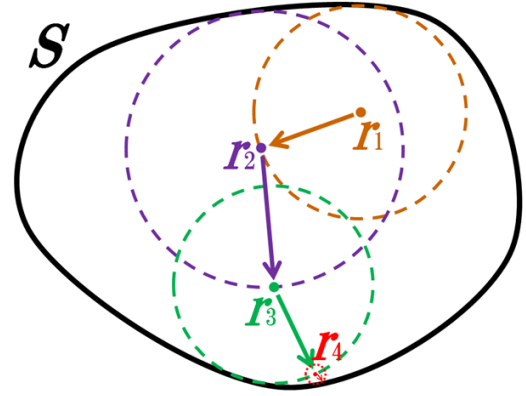(b) For electrostatic fields computed by using `EMS`.

Figure 5: Electric-field enhancement factors as functions of G and Δ.

Figure 6: Two parallel PEC plates with an electric potential difference of 1.0 V. A small groove of the concave structure is made at the center of one plate. The background material is vacuum.

Figure 7: Schematic diagram of FRW. If $r_4 < r_{\min}$, this random walk is terminated, and the potential value at the nearest boundary is used. S indicates a boundary with known potentials.

to Eq. (1), and Eq. (3) is calculated by random walks. Figure 7 shows a schematic diagram of FRW as an example. If r_N is smaller than a certain value ($r_{\min}$), $\phi(X_N, Y_N)$ is set to be the potential value at the nearest boundary. In this study, $r_{\min}$ is set to be 1 nm ($= 10^{-9}$ m).

Letting ϕ_k be an estimate by the k-th single random walk, and performing M random walks in total, we obtain an estimate $\bar{\phi}$ and its error σ of the potential by M random walks according to the following formula:

$$\bar{\phi} = \frac{1}{M} \sum_{k=1}^{M} \phi_k, \quad \sigma = \frac{(\text{Standard Deviation})}{\sqrt{M}}. \quad (5)$$

Advantages of the FRW method are:

1. No meshing, i.e. no space discretization,
2. Simple algorithm,
3. No large amount of memory in computers needed,
4. High parallelization efficiency since this is one of the Monte Carlo methods, and
5. Higher accuracy with larger statistics of random walks.

On the other hand, there is a disadvantage that larger number of computations or operations are needed than in the deterministic methods, such as finite-element, finite-difference, and finite-integration techniques. This disadvantage can be overcome by adopting GPGPU (General-purpose computing on graphics processing units) with many cores, which is a rapidly-advancing field in computer science. It should be noted that GPGPU is weak in complicated algorithms.

In this study, a GPGPU board of NVIDIA Tesla C2070 with 448 cores is used, and a dedicated computer program has been written in `Fortran 2003 / CUDA Fortran` [8] to compute electrostatic potentials with the FRW method. To generate pseudo random numbers, the Mersenne Twister algorithm with a dynamic creation method [9, 10] is implemented in this computer program.

In order to obtain electric fields, potentials at a 0.5μm distance from the conductor surface are computed with an accuracy of 0.00018% using 4032 threads submitted to the GPGPU board. Surface fields are calculated by taking a difference between the computed potentials and 1.0 V divided by 0.5μm, where the corresponding accuracy in electric fields is 0.35%. Typical number of random walks and elapsed time to obtain the above accuracy are $M = 200$ million and 10 seconds, respectively. This computation speed is about five times faster than the same computation with eight threads using dual CPU of quad-core Xeon X5472 (3.0 GHz) (eight cores in total). It should be noted that the computation speed can be made much faster if we use a GPU cluster because the parallelization efficiency is 100% in principle.

Figure 8 shows examples of the computed surface fields, and Fig. 9 shows computation results of the electric-field enhancement factors. All in all, there are good agreements between the results with the FRW method and EMS. However, the results with the FRW method show a few % higher values than the results with EMS.

Benchmark test

In order to demonstrate the validity of the FRW method and its implementation in this computer program, a geometry including an infinitely sharp edge, as shown in Fig. 10, is adopted as a benchmark. For the geometry, exact potential values can be calculated according to the following formula:

$$
|\vec{E}(X,Y)| = \left| \frac{dw}{dz} \right| \tag{6}
$$

$$
z = \frac{b}{\pi} \left(\ln \frac{1 + \sqrt{1 + e^{-(\pi/\phi_0)w}}}{1 - \sqrt{1 + e^{-(\pi/\phi_0)w}}} \right.
$$
$$
\left. -2\sqrt{1 + e^{-(\pi/\phi_0)w}} \right) + ib \tag{7}
$$

where $\vec{E}(X,Y)$ indicates a two-dimensional electrostatic field vector, $z = X + iY$, $w = u + i\phi(X,Y)$, $\phi_0 = 1.0$ V, and $b = 1.0$ mm. Eq. (7) is a $z - w$ transformation, which can be derived by using the Schwarz-Christoffel mapping for the geometry shown in Fig. 10.

Figure 11 shows results of the computations by using EMS and the FRW method. While the results with the FRW method are perfect, the results with EMS show undershoot toward the edge in the region of $X \lesssim$ (mesh size). The undershoot can be attributed to the meshing effects in EMS; FRW is a mesh-free method.

CONCLUSIONS

Electric-field enhancements due to fine concave structures with the $R = 50\mu$m round chamfer have been computed with the three different methods: the FIT-based RF-field simulation by using MWS, the FIT-based static-field simulation by using EMS, and the FRW (mesh-free and
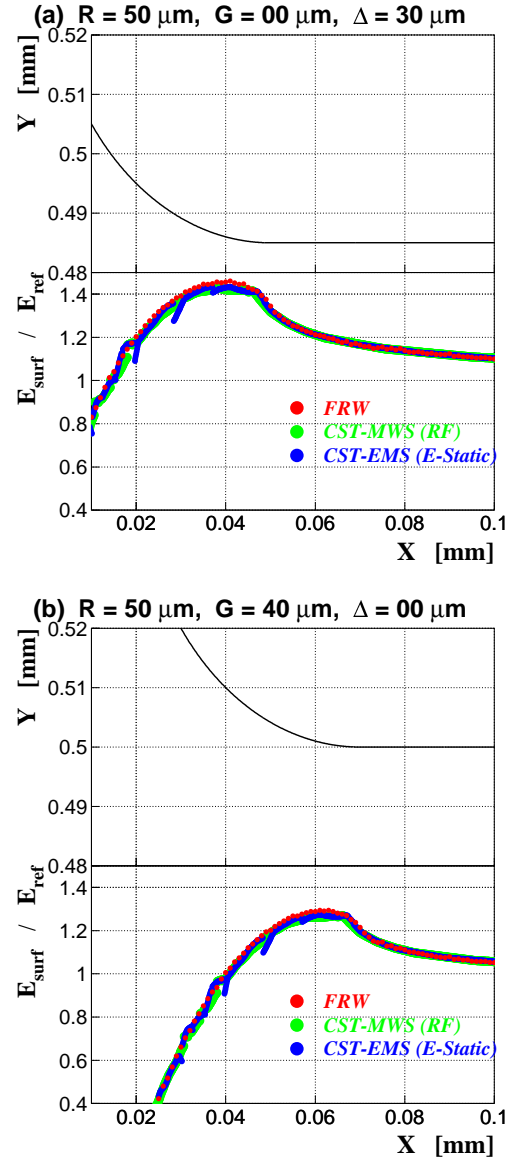

Figure 8: Conductor surfaces (top figures) and the surface electric-field strengths as a function of X (bottom figures). Each red point indicates a computation result using the FRW method.

stochastic). There are agreements among the three methods within a few % accuracy, where the results by MWS and EMS show a few % smaller values. It has been found that there is at least 20% enhancement even with no gap and $\Delta = 0$, and the enhancement increases to 40% as the Δ size increases to 25μm.

It has been demonstrated in this study that the FRW method gives high-precision calculations of local fields, and it is practical and promising because of its suitability for GPGPU computing. It should be emphasized that this FRW method is applicable to any structure. The next step is to apply this FRW method to computations of surface-field enhancements on conductor surfaces damaged by break-
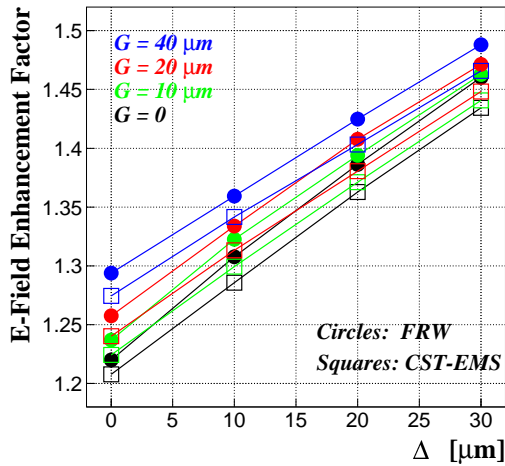
Figure 9: Electric-field enhancement factors as functions of G and Δ. The circles (squares) indicate computation results by using the FRW method (EMS).
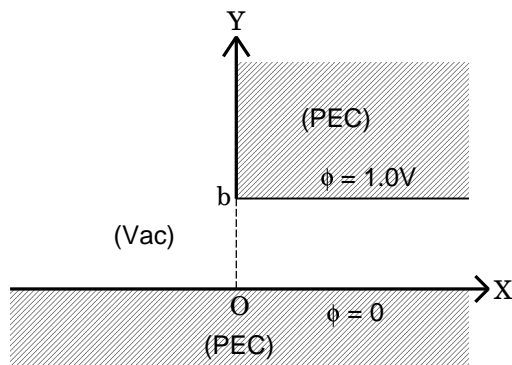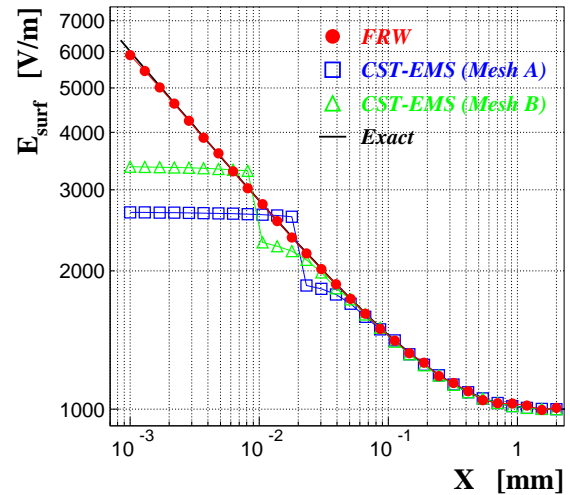

Figure 11: Surface electric-field strengths at $Y = b$ as a function of X for the benchmark geometry shown in Fig. 10. Near the infinitely sharp edge located at $(X, Y) = (0, b)$, the mesh sizes in the Mesh A and B of the EMS computations are $36\,\mu$m and $18\,\mu$m, respectively. The solid line indicates an exact solution from the analytical formulae of Eq. (6) and (7).

Figure 10: Geometry for the benchmark test. The hatched and white areas indicate PEC and vacuum regions, respectively. There is an infinitely sharp edge at $(X, Y) = (0, b)$. The minimum distance and potential difference between the two PEC regions are set to be $b = 1.0\,$mm and $1.0\,$V, respectively.

down and/or discharge in accelerating structures, where such surface profiles can be measured with laser-scanning or atomic-force microscopes.

ACKNOWLEDGMENTS

REFERENCES

[1] Toshiyasu Higo *et. al*, "FABRICATION OF A QUADRANT-TYPE ACCELERATOR STRUCTURE FOR CLIC," presented in EPAC08, Genoa, Italy, 2008, PaperID: WEPP084.

[2] Thomas Weiland and Rolf Schuhmann, "Discrete electromagnetism by the Finite Integration Technique," The Japan Society Applied Electromagnetics and Mechanics, Vol. 10, No. 2, 2002.

[3] CST STUDIO SUITE version 2011.04 is used in this study.

[4] http://www.cst.com/

[5] Perfect Boundary Approximation$^{\text{TM}}$

[6] Matthew N.O. Sadiku, "Monte Carlo Methods for Electromagnetics," CRC Press, 2009.

[7] The potential ϕ is a solution of Laplace equation, i.e. a harmonic function.

[8] http://www.pgroup.com/doc/pgicudaforug.pdf .

[9] Makoto Matsumoto and Takuji Nishimura, "Mersenne Twister: A 623-Dimensionally Equidistributed Uniform Pseudorandom Number Generator," ACM Transactions on Modeling and Computer Simulation, Vol. 8, No. 1, 1998, pp 3-30.

[10] Makoto Matsumoto and Takuji Nishimura, "Dynamic Creation of Pseudorandom Number Generators," Monte Carlo and Quasi-Monte Carlo Methods 1998, Springer, 2000, pp 56-69.